Cross-sectional stability of aluminium extrusions with arbitrary cross-sectional shapes – experimental and numerical research

[1] J. Mennink

   TNO Building & Construction Research, Delft, The Netherlands

   Eindhoven University of Technology, Eindhoven, The Netherlands

[2] F. Soetens

   TNO Building & Construction Research, Delft, The Netherlands

   Eindhoven University of Technology, Eindhoven, The Netherlands

[3] H.H. Snijder

   Eindhoven University of Technology, Eindhoven, The Netherlands

Aluminium extrusions applied in daily practice are often thin-walled with complex cross-sectional shapes. These shapes are based on a variety of demands that are in general non-structural. As a result, several types of instability may occur, including overall and cross-sectional instability modes as well as mode interactions. Research on overall buckling is usually based on simple and symmetrical cross-sections, whereas cross-sectional instability is simplified to buckling of individual plates. It is therefore highly unlikely that these design rules provide an accurate description of the actual buckling behaviour of arbitrary cross-sections. As predicted failure modes not necessarily agree with actual ones, the outcome of the results may be overly conservative but could be unsafe as well. This article provides a summary of results and insight obtained from an extensive experimental and numerical program executed, Mennink (2002). These results shed a new light on the actual buckling behaviour of members with non-standard cross-sections.

Key words: stability, aluminium, local buckling, extrusions, distortional buckling, buckling

1   Introduction

1.1 Aluminium extrusions in structural applications
Aluminium extrusions are widely used in structural applications and transportation. This includes load-bearing structures, roof claddings, helicopter platforms, bridges, and greenhouses, as well as trucks, trains, ships and airplanes. The choice for aluminium almost always derives from its flexibility, as material and shape can be designed to match the requirements of any situation.

Three key aspects exist to apply aluminium. First, its low unit mass (one third of steel) allows a

substantial weight reduction compared to other materials like steel, thus increasing the allowable live load and reducing assembly, and transportation costs. Secondly, when exposed to air, aluminium immediately forms a tight oxide-layer. Thus, most alloys are not susceptible to ongoing corrosion, even in extreme environments. For example, aluminium has been used successfully on offshore platforms for decades without the use of protective layers. Finally, the extrusion manufacturing process provides an almost infinite range of possible cross-sectional shapes, as shown in figure 1. Designers can thus freely optimise the cross-section by adding functions like e.g. stiffeners and weld backings, or to accommodate connections.
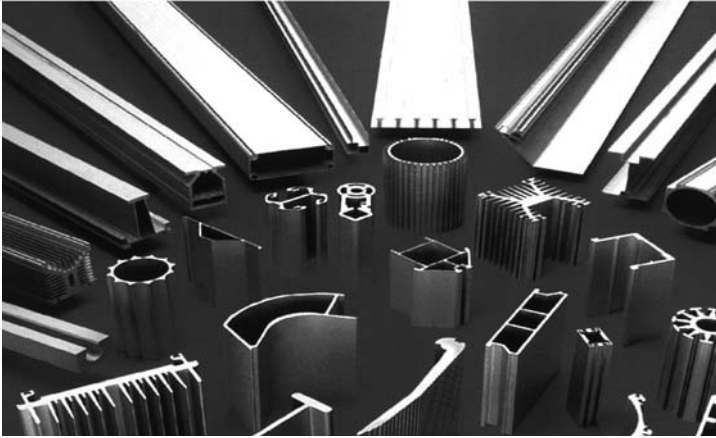

Figure 1: Examples of complex aluminium extrusions

These positive aspects show a very useful material. However, aluminium also has some less positive aspects. The modulus of elasticity ($E = 70000 \text{ N/mm}^2$) of aluminium is only one third of that of steel. Thus, more material is necessary to satisfy stiffness criteria. In addition, it makes aluminium more susceptible to instability (buckling). Secondly, high temperatures reduce the material strength and nullify heat-treatments. Weld design and fire resistance can therefore become key aspects. Finally, the costs per kilogram of aluminium are higher than those of steel are. Though these negative aspects seem rather demanding, they can be accounted for by taking optimal advantage of the freedom of cross-sectional shape. Optimisation, i.e. minimising of cross-sectional area or inclusion of additional functions, is thus an important part of the design process. For example: extruded stiffeners can prevent stability problems, optimisation can minimise the cross-sectional area, while welds can be relocated to less stressed areas. Thus, optimisation is an important part of the design process. In practice, it often results in thin-walled extrusions with complex cross-sectional shapes.

*1.2 **Buckling of axially compressed aluminium extrusions***

The combination of complexly shaped thin-walled cross-sections and a moderate material stiffness (Young's modulus *E*) results in cross-sectional instability as one of the decisive design issues for aluminium extrusions. Cross-sections susceptible to this type of instability often consist of slender plates that are connected at nodes. Two examples are presented in figure 2. It can be seen that while some connecting nodes remain in place, others translate when instability due to compressive stresses occurs. As this may cause a significantly different behaviour, a distinction is made between local and distortional buckling:

- *Local buckling* refers to buckling patterns where each connecting node between plate segments of a section remains in place.
- *Distortional buckling* refers to buckling patterns where at least one connecting node between plate elements translates.

undeformed

deformed

Distortional buckling   Local buckling
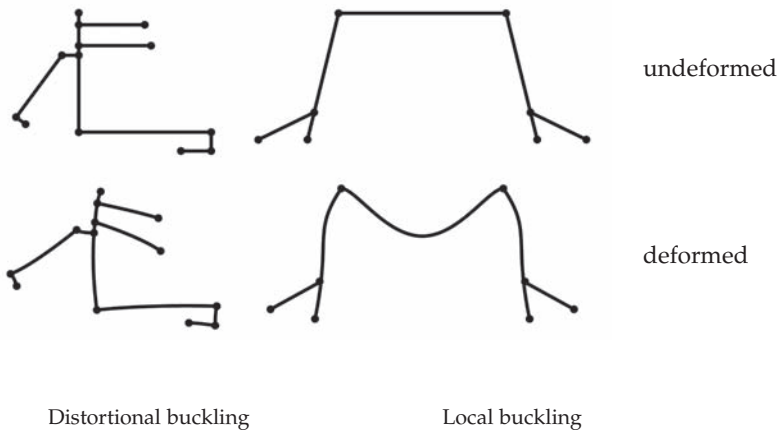
Figure 2: Cross-sectional instability – Local and distortional buckling

Design rules for local buckling of cross-sections (see e.g. Eurocode 9 (CEN 1999)) are based on the theoretical solutions of the plate-buckling problem, which are subsequently fitted empirically to test results. Though this approach has proven itself for traditional cross-sections like e.g. rectangular hollow sections, I- and U-sections they do not represent the actual behaviour as they neglect plate interactions.

Design rules for distortional buckling are limited to a few specific cases like: flanges with edge stiffeners and webs with one or two intermediate stiffeners. Though steel design codes like Eurocode 3 (CEN 1993) provide design rules for some additional geometries, these rules tend to become very complicated and time-consuming with an increasing complexity of the cross-sectional shape.

In addition to the individual modes, interaction between local and overall buckling is hardly investigated, but rather drastically incorporated (see e.g. Mennink (2002)). Again, research is limited to traditional cross-sections. Thus, it can be concluded that the existing design rules for instability are limited with respect to cross-sectional instability; only a very limited range of cross-sections is covered and only with a limited accuracy. The contrast with the complexity of cross-sections used in practice is manifest. Without validated and safe design rules, daily practice might lead to disturbingly inaccurate and even unsafe design for complex aluminium cross-sections under compression.

2   Experimental investigation of cross-sectional stability

This chapter presents a summary of existing experimental work and reports on the work executed within the PhD-study of J. Mennink (2002). Specific attention is paid to a wide range of non-traditional cross-sections.

2.1 Summary of existing experimental work

A large test program on square hollow sections (SHS), rectangular hollow sections (RHS) and U-sections (US) was executed at Salerno University, Italy (figure 3). The aim of these tests was to determine and validate the design rules of the Eurocode 9 (CEN 1999). See e.g. Landolfo et al. (1999) and Mazzolani et al. (1998).

The complete experimental program deals with specimens made of the 6000 and the 7000 series alloys. In addition, different tempers have been considered. Two types of RHS members can be recognized, RHS with sharp corners and RHS with rounded corners. Note that one specimen (RHS27) has an intermediate plate element stiffening the largest side of the cross-section.
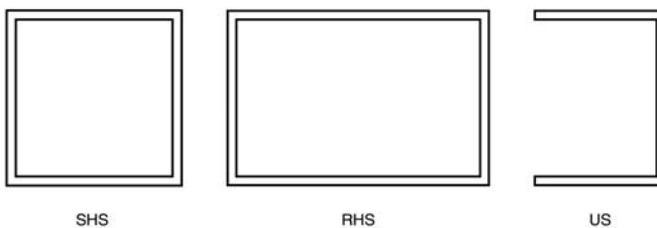

Figure 3: Cross-sections tested in the Salerno program

The Helsinki program (Hassinen 2000) aimed at verification of the Eurocode 9 by providing additional data on more complex sections (figure 4). It consists of: 17 RHS, 19 angles and 6 RHS-specimens with openings of aluminium alloy 6063 T6. The length of the specimens was varied in order to cover the slenderness ratios used in practice. The edges of the specimens

were completely fixed within the frame of the testing machine. The specimens were loaded in uniform compression.
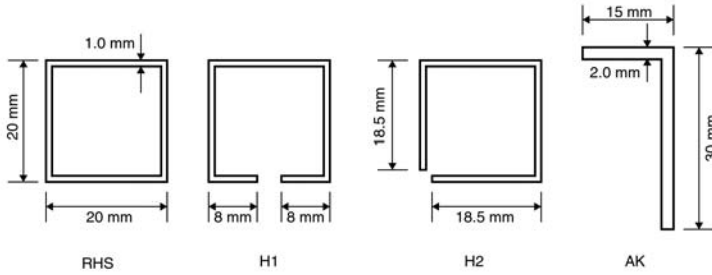

Figure 4: Cross-sections tested in the Helsinki program.

2.2 *Eindhoven experimental program*

The Eindhoven test program (Mennink, 2002) consists of three series of uniformly compressed aluminium extrusions. The material was specified as AlMgSi0.5 (6063-T6). Subsequent series regard: RHS, US and complex sections (CS). The tests are explained more in detail in the following sections.
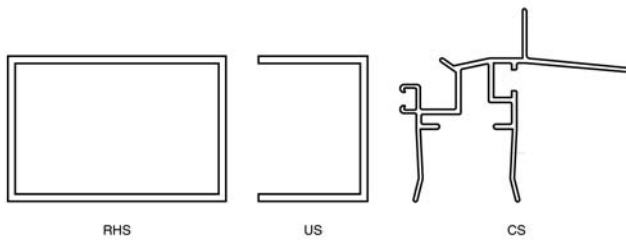
Figure 5: Examples of cross-sections tested in the Eindhoven program

2.2.1 Rectangular hollow sections (RHS)

The first test series consists of 17 compression tests on rectangular hollow sections (RHS). The aim of these tests was twofold: first, to determine the accuracy of the applied test set-up by variation of support conditions and specimen length. Secondly, the aim was to obtain experimental data on local buckling of internal plates (webs) while taking the influence of connecting plates into account.

2.2.2 U-sections (US)

The second test series consisted of 21 compression tests on US specimen. The specimens were obtained from RHS by cutting. The aim of this series was to obtain experimental data about local buckling of outstands (flanges), including the stiffening influence of a connecting internal plate element (web). US specimen have two characteristic aspects. First of all, as the critical length of outstands is much larger than its plate width one would need very tall specimen to obtain more than one buckle over the specimen length. Secondly, flange buckling of US specimens may result in such a reduction of overall bending stiffness that in order to prevent the occurrence of overall column buckling one would need very compact, short, specimens. As these two aspects contradict, it is almost impossible to accommodate both. Moreover, it is very hard to determine in advance the influence of even one aspect. Therefore, it was chosen to use a constant, arbitrary chosen, specimen length of L = 300 mm. Though the influence of support conditions as well as overall buckling may both still occur, this approach highly simplified the test set-up and thus enhanced the quality of the execution.

2.2.3 Complex sections (CS)

The third test series consisted of 40 tests on extrusions with 12 types of complex cross-sectional shapes (CS). The specimens were obtained from commercially available extrusions used mainly in greenhouses. The aim of these tests was to obtain experimental data on the cross-sectional instability behaviour of cross-sections that cannot be investigated by the current design codes. Well over a hundred cross-sections were studied in advance to determine the appropriateness of these specimens with respect to cross-sectional instability. The finite strip program CU-FSM allowed the determination of the critical stresses for cross-sectional and overall instability. The twelve cross-sections were chosen on the basis of their critical stress being substantially less than the 0.2% proof stress. Their cross-sections are presented in figure 6. Various specimen lengths were determined in order to obtain either solely cross-sectional instability or interaction with overall buckling modes.

CS01   CS02   CS03

CS04   CS05   CS06

CS07   CS08   CS09

CS10   CS11   CS12
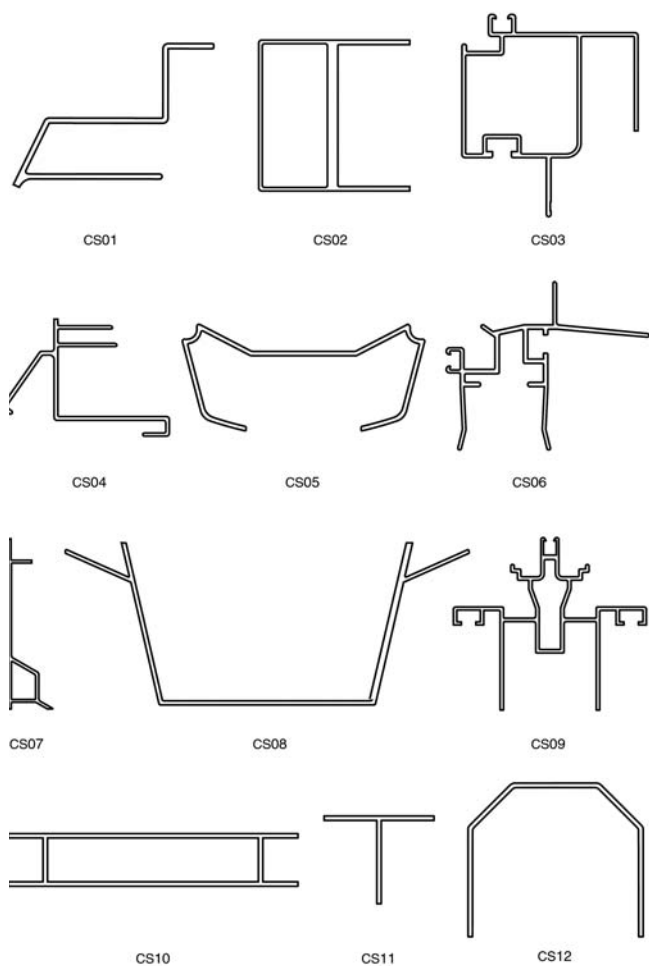
Figure 6: Complex sections (CS) tested in the Eindhoven program

2.3 *Test set-up Eindhoven experimental program*

The test set-up used in the Eindhoven experimental program is presented in figure 7. The specimens are placed, freely, between fixed supports. Thus, the specimens resemble clamped columns that are loaded into compression by a uniform axial end displacement.

The tests have been executed on a 250-kN bench. The bench is operated in displacement control of the hydraulic cylinders, which are steered by the measurement of the axial shortening of the specimens. Two perfectly flat support plates were fixed to the test rig; their flatness and parallelity was verified with an accuracy of 0.01 mm. The specimens were placed freely in between these plates. Double layers of Teflon were applied in-between the RHS-specimen and the support plates, in order to minimise friction and thus obtain an almost undisturbed displacement field. Thus, Teflon led to a remarkable improvement of the results of specimens

that failed through squashing. Unfortunately, the reduction of friction also allows the occurrence of slip. As a result, the overall buckling length increased from half the specimen length to the entire specimen length. Thus the overall buckling resistance dropped substantially and could often become decisive. Therefore, Teflon was not applied in the tests on US- and CS specimens.
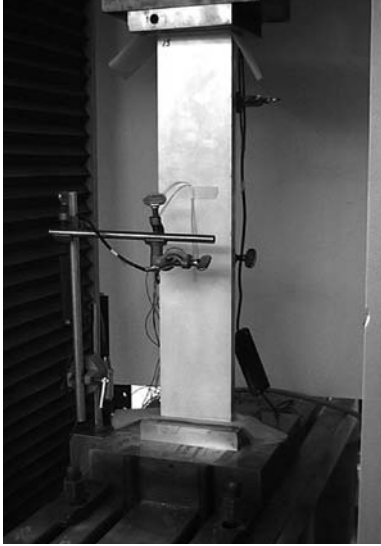

Figure 7: Test set-up compression tests Eindhoven program

In order to obtain uniform axial shortening, both edges of the test specimens have to be flat, as well as parallel to each other. The RHS as well as the US specimen have been machined with an accuracy of 0.01 mm. Despite the effort on accuracy, some edges still showed a few small wires from the machining. Therefore, the spark erosion process was used to obtain flat edges for the complex sections. This process resulted in an even more accurate flatness (no wires, accuracy of 0.005 mm). However, the resulting parallelity of the edges was, for the larger specimens, substantially less and resulted for some cases even in visual gaps in the order of 0.1 mm.

2.4 *Imperfection measurements*

To obtain more insight into the actual imperfections, extensive measurements were performed on the initial deflections of the CS-specimen. A computerized bench was used to accurately measure the flatness of each plate of a cross-section, see figure 8. Each specimen was placed on the bench and the flatness of each plate was measured for a large number of points.
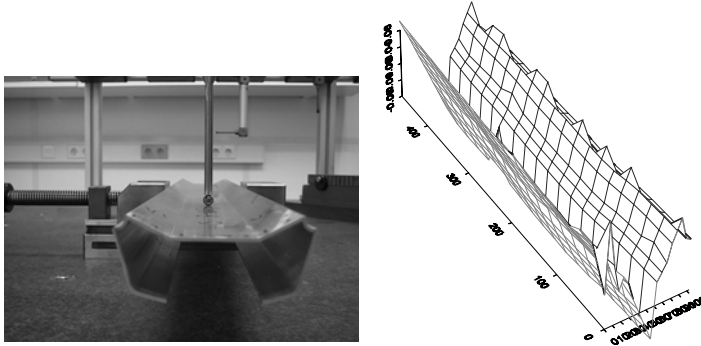
Figure 8: Set-up and characteristic results of imperfection measurements – Specimen CS05

An example of the measured deformation pattern is given in figure 8, showing a "dent" over the entire specimen length. Such a dent acts like a kink and therefore results in a limited improvement of the buckling strength of the plate, which contradicts the common assumption that imperfections reduce strength.

Imperfection patterns may be characterised by their shape and amplitude. Chapter 3 will explain that the finite element analyses apply imperfection shapes according to the deflected shape of the first Eigenmode of the specimen. Thus the imperfection measurements have been elaborated in Mennink (2002) to provide the amplitude of the first Eigenmode, denoted by e_0.

2.5 Material characteristics / tensile tests

Tensile tests were executed according to NEN-EN 10002-1 (NNI 1991) to determine the material characteristics. As these are used as input for finite element analyses of chapter 3, the actual stress-strain relation in both the elastic and inelastic ranges have to be determined accurately. This includes the modulus of elasticity E, and the 0.1% and 0.2% proof stresses $f_{0.1}$ and $f_{0.2}$. The tests have been executed using various load cycles in the elastic range and strain gauges on both sides of the specimen.

The results of the tensile tests show a remarkable consistent value of E (66 kN/mm²). This is substantially lower than the generally used value of 70 kN/mm² (bandwidth of 68 to 72). This shows that it is essential to execute tensile tests with at least one load cycle.

2.6 Failure modes

The compression tests show a wide range of instability modes, as well as various types of interactions. Examples are given in figure 9. Note that a distinction must be made between the deformation mode at buckling initiation (e.g. local buckling) and the one that causes failure (e.g. flexural buckling). The results have been categorised using the following notations:

• Squashing (S)
• Flexural buckling (F)

- Torsional (T) and flexural-torsional (FT) buckling
- Local buckling (L)
- Distortional buckling (D)
- Interaction of local and flexural buckling (L/F)
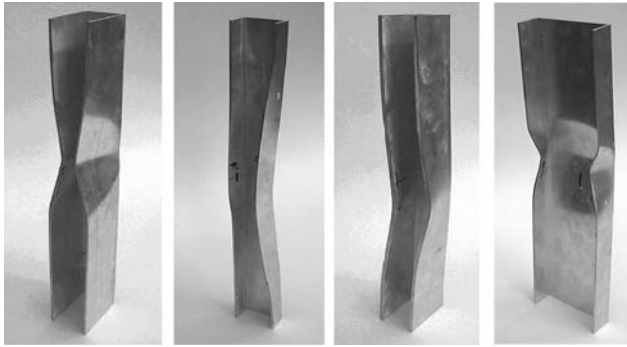
| US04 (L) | US01 (L) | US14 (FT) | US10 (L/F) |

Figure 9: Characteristic failure modes of US-specimens

2.7 *Axial strength and stiffness*

The experimentally determined load-displacement curves relate the measured reaction force (N) to the applied axial shortening (u), as presented in figure 10A. However, to obtain comparable results the N-u diagrams are replaced by stress-strain diagrams as presented in figure 10B. These diagrams relate the average axial stress σ_{av} (=N/A) to the average axial strain ε_{av} (u/L).
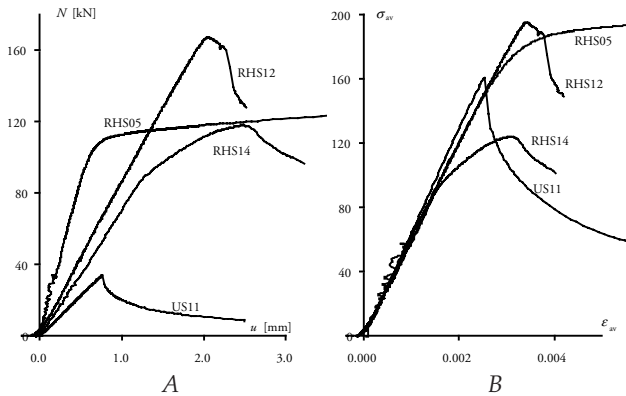

Figure 10: Characteristic load-displacement and stress-strain diagrams, Eindhoven program

The curves presented in figure 10B are representative for the possible failure modes, as explained below. Two representative loads can be determined: the load at initial buckling N_{cr}

(e.g.87.1 kN for RHS14), and the ultimate or failure load N_u. Initial buckling is only relevant in case of local or distortional buckling (e.g. RHS14).

• Squashing (S)

  The behaviour of a an accurately executed compression test on compact cross-sections (RHS05) resembles that of a tensile test. However, out-of-plane deformations will occur suddenly at substantial plastic strains.

• Flexural (F) or flexural-torsional (FT) buckling

  If the dominant failure mode is overall buckling (RHS12, US11), the load-displacement curve shows little deviations from the elastic curve up to the ultimate load. Though column failure is usually associated with a smooth top of the load-displacement curve (RHS12), most specimens fail with a sharp peak (US11).

• Local (L) or distortional (D) buckling

  Sections susceptible to cross-sectional instability (RHS14) approach linear-elastically the bifurcation load N_{cr}. Subsequently, these cross-sections progress gradually into inelastic failure, which can be governed by overall buckling.

Additional information can be found from the results of the strain gauges. These were applied at mid-length of the specimen, one at each plate. Results for two representative specimens are presented in the diagrams of figure 11. These diagrams, for RHS14 and RHS07, include four strain gauges in grey; for RHS14 also the average result of the LVDT is presented in black.
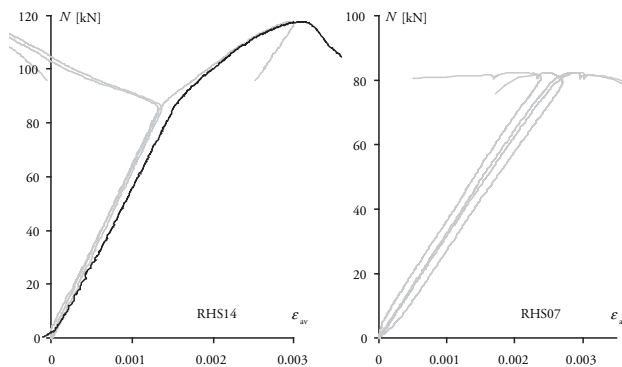
Figure 11: Characteristic load-strain curves: (strain gauges in grey, LVDT in black)

For RHS14 the strain gauges show identical results up to the bifurcation load (N_{cr} = 87.1 kN), indicating uniform compression. Contrarily, the horizontal gap between the curves for RHS07 indicates load eccentricity. Assuming linear elastic theory, the horizontal difference $\Delta\varepsilon$ (arbitrarily determined at a quarter of N_u) between the curves can be used to obtain an indication of the difference in axial stress over the cross-section.

In general, LVDT's show a less stiff behaviour than the strain gauges do. This is caused by the more accurate measurement of the strain gauges as well as the influence of inaccuracies during load initiation.

The stiffness of the load-strain curves has been analysed in Mennink (2002) as the compression stiffness E_c and is, together with $\Delta\sigma$ ($=E * \Delta\varepsilon$), summarised in chapter 4. It is concluded that the deviation between the stiffness of the representative tensile tests and the compression tests is small.

3   Numerical work

This chapter presents the validation of a finite element (FE) model, with respect to the cross-sectional stability behaviour of aluminium extrusions. Therefore, FE-analyses have been executed on almost all tests executed within the Eindhoven experimental program, as described in chapter 2.

3.1 Executed FE-analyses

As specified in 2.2, the Eindhoven experimental program consists of compression tests on 17 RHS, 21 US and 40 tests on CS specimens. However, tests RHS01, RHS02, RHS04, RHS17, and RHS19 failed through squashing. Tests RHS15 and RHS16 have a varying plate thickness as well as internal radii. Tests CS09-1 to CS09-3 have very complex cross-sections, and thus inaccurate cross-sectional properties, while no tensile test was executed. All these tests have not been analysed. This leaves a total of 68 tests that have been simulated numerically.

The applied dimensions used in the FE-simulations, see Mennink (2002), are taken as closely as possible to those actually measured.

3.1.1 Applied imperfections

Four major types of geometrical imperfections may occur: initial deflections or curvature, load eccentricities, eccentricities due to asymmetric cross-sections, and thickness deviations.

Initial deflections and curvatures are characterised by their shape and amplitude e 0. However, most imperfection measurements are not accurate enough to determine the shape of the imperfection pattern. Therefore, in agreement with common practice, the deformation pattern belonging to the lowest positive Eigenvalue of the specimen is applied for the shape of the imperfection pattern. The measured imperfections are used to determine the amplitude. Note that though some overall buckling phenomena may be very susceptible to small imperfections, cross-sectional instability –which is focussed upon- is not that susceptible.

Load eccentricities (represented by $\Delta\sigma$) were measured in the experiments (see section 2.7). However, it is not known if these are caused by leaning, crookedness of the column, or due to non-parallelity of the loaded edges. Therefore, the influence of this deviation is not accounted for in the FE-analyses. As some of the experiments show substantial load eccentricities, they

partially explain the deviations between the experimental and finite element results. The influence of asymmetrical cross-sections and thickness deviations is accounted for by the application of the actually measured geometry and measured plate thicknesses. Note that the accuracy of the thickness measurement, as well as the accuracy of the extrusion process, reduces with decreasing plate thickness.

3.1.2 Applied material characteristic

The stress-strain curves of the tensile tests are applied as material characteristic in the FE-analyses. The analyses are executed using a Von Mises yield criterion and a work-hardening stress-strain relation. The used procedure is described in Mennink (2002). It was also found that the accuracy of the stiffness (E) from tensile tests, as presented in literature, is rather limited (5-10%). While both the buckling stress and post-buckling stiffness are linearly related to E, it is an important parameter to consider in comparing experimental and numerical results.

3.2 Set-up finite element model

3.2.1 Mesh

The test specimens are simulated using a mesh of so-called curved shell elements. Each part of the test specimen is modelled as a rectangular plate, which is divided into rectangular elements. An example is shown in figure 12.
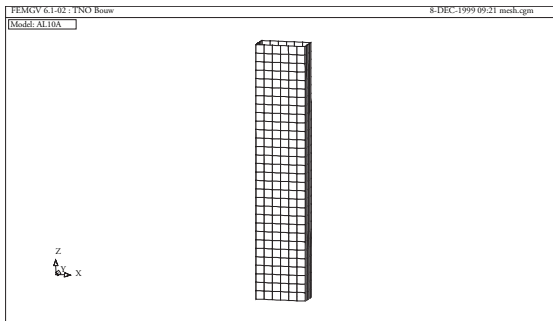
Figure 12: Mesh schematisation of specimen RHS10

The specimens are modelled in DIANA (Witte et al. 1996), using CQ40S eight-node quadrilateral iso-parametric curved shell elements, which are based on quadratic interpolation and a 2*2 point Gauss integration scheme over the element area. Straight normals are assumed, but not necessarily normal to the reference surface. Transverse shear deformation is included according to the Mindlin-Reissner theory. The elements present a reduced deformation pattern. Instead of 6 degrees of freedom, each node has three translations as well as two rotations, thus

resulting in forty degrees of freedom per element. Typically, the strain ε_{xx} varies quadratic in x-direction and linear in y-direction, while the strain ε_{yy} varies linear in x-direction and quadratic in y-direction. Application of seven thickness integration points in each of the Gauss points provides sufficiently accurate results. This is necessary to accurately describe a non-linear stress distribution over the plate thickness.

3.2.2 Mesh density

Essential in the determination of the mesh density is the description of the (in-) elastic out-of-plane deformation of buckles. The CQ40S-elements are able to accurately describe a quadratic deformation (deflection) pattern. For sine-shaped deflections, according to elastic buckling analyses, it would be sufficient to apply two elements for each half-sine. However, as inelastic stresses are determined only at the Gauss integration points, more elements and integration points are necessary to describe the plastic deformations of a buckle.

Based on a parameter analysis it was concluded to use a 6*6 mesh for each buckle in the RHS and US analyses. For the complex sections (CS) the mesh density was reduced from a 6*6 mesh to a 4*4 mesh, as the total number of plates within these cross-sections would otherwise result in an overly large number of elements. Nevertheless, all slender plates were attributed six elements over the plate width, whereas compact plates received only two. The number of elements in axial direction is based on the number of elements resulting from the application of the 4*4 mesh for each buckle, or that of an arbitrary chosen element length-width ratio of 3. For each specimen the mesh density is summarised in Mennink (2002).

3.2.3 Support / loading conditions

In the experiments, the specimens are positioned on steel support plates, as explained in section 2.3. Though this resembles a fixed end support, it is based on friction only. Nevertheless, parameter analyses concluded that the influence of the support conditions is negligible for specimens with sufficient length or if buckling occurs in the elastic range.

As Teflon-layers were applied, the RHS tests have been simulated using supports that allow the edge cross-sections to expand and translate, but prohibit any rotations as well as axial deformations. Contrarily, Teflon-layers were not applied at the US and CS-specimens. Though slip between specimen and support plate might have occurred, it has not been observed. Therefore, all translations and rotations have been restricted at the supported edges of the US and CS-specimens.

3.2.4 General calculation procedure

The finite element analyses were executed according to the DIANA code, release 7.2 (Witte et al. 1996). The analyses are divided into three steps, which are performed respectively by the DIANA modules: LINSTA, EULER and NONLIN. The first module, LINSTA, is used for linear elastic analysis under static circumstances. This module is essential as a preliminary analysis for the stability and geometrical and physical non-linear analyses.

The stability analysis (EULER) results in a set of sequential buckling modes. Each mode belongs to a buckling load and has its own deformation pattern. The deformation pattern of the first Euler buckling mode is used as imperfection pattern for the geometrical non-linear analysis, as explained in section 3.1.1. Geometrical and physical non-linear analyses (NONLIN) require input from the LINEAR and EULER analyses; the physical non-linear behaviour is described using the actual material characteristic.

In physical and geometrical non-linear analyses, the influence of the load step size can be significant. The axial shortening (u) of the specimen is applied as a uniform edge displacement of the top cross-section of the test specimen. The size of the load steps depends on two considerations. First, the accuracy increases with smaller load steps, especially when physical non-linear behaviour occurs. In case of sudden changes in the mechanical behaviour (development of a buckle), large load steps could even lead to failure of the numerical process. The second, more practical, consideration is that results are obtained only at the load steps; small load steps are required to obtain detailed information. The size of the load steps (Δu) has been chosen such that the resulting curves of the load-deflection diagram are fluent; see e.g. figure 14. Parameter analysis has proven this approach to be sufficiently accurate.

3.3 **Results FE-analyses**

3.3.1 Deformation patterns and failure modes

Figure 9 presented examples of the deformed specimen of the experiments. Figure 13 presents the according deformation patterns of the FE-analyses at the failure load. It also includes the specification of the test specimen and failure mode. Comparison of the numerial deformation patterns to the experimental ones shows that the failure modes are identical.

RHS05 (S) RHS14 (L) RHS12 (F) RHS09 (L/F)

US04 (L) US01 (L) US14 (FT) US10 (L/F)

CS10-3 (L) CS05-3 (D) CS11-2 (T)
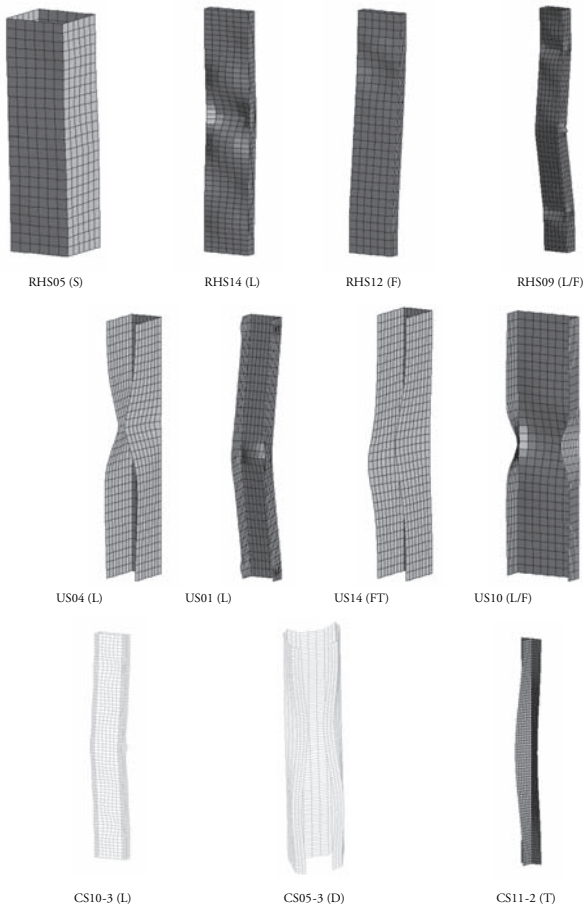
Figure 13: Deformations at failure – FE-results

3.3.2 Axial strength

Three characteristic strength-strain curves could be determined, each referring to a type of failure: squashing, overall buckling, and cross-sectional instability. Overall buckling and cross-sectional instability are explained respectively by the results of US10 and CS11-2.

The results for specimen US10 are presented in figure 14. The load-displacement (N-u) diagram presents the experimental result, two curves with FE-results using different imperfections. For comparison it includes the material, which represents the engineering stress strain curve multiplied with respectively, the cross-sectional area and specimen length. The load versus out-of-plane deflection (N-w) diagram presents the FE-results as well as the experimental failure load ($N_{u;exp}$). The experiment fails through flexural buckling with a distinct peak, which is associated with small imperfections. Therefore, two FE-analyses have been executed,

representing the actual and small imperfections by using imperfection amplitudes e_0 of respectively 0.12 and 0.01 mm. The difference in failure loads of the FE-analyses (12%) shows the distinct influence of imperfections on flexural buckling. Note that subsequent sections present the results based on using the actual imperfections.
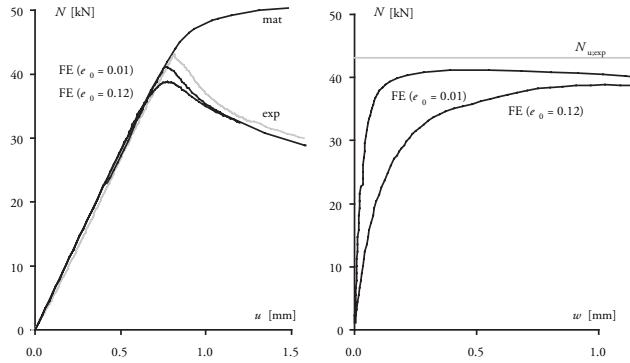
Figure 14: Experimental and numerical load-displacement and load-deflection curves (US10)

The T-section (CS11-2) shows behaviour associated with local buckling, see figure 15. The specimen buckles at the bifurcation load N_{cr} and shows a substantial amount of post-buckling strength. Failure occurs due to the interaction with flexural buckling. It is noted that there is no clear distinction between flange-buckling and torsional buckling. There is a good agreement between experimental and numerical results.
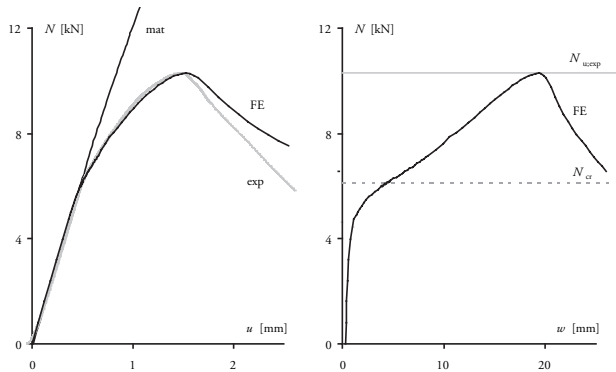
*Figure 15: Experimental and numerical load-displacement and load-deflection curves (CS11-2)*

3.3.3 Axial stiffness

In general, no distinction is made between the material characteristics of aluminium alloys under tensile or compressive forces. Therefore, the results in the elastic range of the compression and tensile tests should be comparable. Furthermore, the tangent stiffness of the

post-buckling range is an important parameter in the determination of the post-buckling behaviour of plates. To illustrate this, figure 16 presents for specimen CS11-2 the tangent stiffnesses (E_T) of the tensile test, the compression test (both strain gauges and LVDT's), and that of the FE-analysis. The resulting curves show excellent agreement. A value for the "compressive" modulus of elasticity (E_c) is determined based on the elastic results of the strain gauges. The figure also shows that plate buckling results a stiffness reduction, and that the results of the finite element analyses largely agree with that of the LVDT's. Note: as the strain gauges are positioned locally on a buckled specimen, their results are not comparable to that of the FE-analysis.
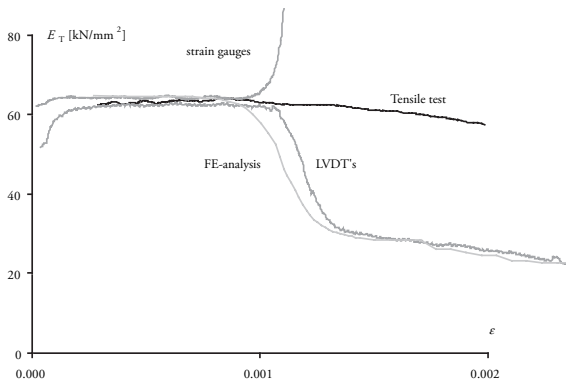
Figure 16: Comparison of the tangent stiffnesses of the compression test (strain gauges and LVDT's), tensile test and FE-analysis (CS11-2)

4   Comparison of experimental and numerical results

The results of the FE-analyses and experiments executed within the Eindhoven program are summarised in he following two tables. These are used to validate the FE-model to the experiments.

4.1 Summary of results

The following tables present the experimental and FE-results for the RHS- and US series, respectively the CS-series. These results consist of: the experimentally found load eccentricity ($\Delta\sigma$), the compression stiffness (E_c), the bifurcation and failure loads (N_{cr} and N_u) and their modes, as well as the tensile load (N_t) at which tensile forces occur at the supports. Finally, the rightmost columns compare the bifurcation and ultimate loads. If bifurcation occurs in the experiment, the value of $N_{cr;FE}/N_{cr;exp}$ is presented. With respect to failure the lowest value of $N_{u;FE}/N_{u;exp}$ or $N_{t;FE}/N_{u;exp}$ is presented.

RHS	EXP						FEM						FE / Exp	
			Bif.		Failure			Bif.		Failure			Bif.	Fail.
Spec.	$\Delta\sigma$	E_c	Md.	N_{cr}	Md.	N_u	E_c	Md.	N_{cr}	Md.	N_u	N_t	Bif.	Fail.
RHS01	29.0	69.9			S	130.1								
RHS02	8.1	68.6			S	129.7								
RHS04	12.3	67.1			S	125.1								
RHS05	12.0	67.9			S	128.5	65.3	L	600.3	S	121.5			0.95
RHS06	6.8	70.8			L	83.8	66.4	L	92.5	L	86.9			1.04
RHS07	19.9	70.6			L	82.2	66.4	L	89.6	L	84.9			1.03
RHS08	14.5	69.5			L	86.5	67.1	L	87.0	L	83.1			0.96
RHS09	5.8	70.0			L-F	84.2	66.3	L	83.0	L-F	83.0			0.99
RHS10	8.8	68.0			L	173.3	66.4	L	216.1	L	172.4			1.00
RHS11	23.4	67.7			L	159.8	66.5	L	210.6	L	164.6			1.03
RHS12	0.6	69.4			L-F	167.2	67.5	L	190.2	L-F	163.8			0.98
RHS13	15.8	74.2			L-F	173.3	67.5	F	163.6	F	141.4			0.82
RHS14	3.3	65.1	L	87.1	F	117.6	64.1	L	78.7	L-F	131.7		0.90	1.12
RHS15*	3.4	70.1			F	85.2								
RHS16*	8.0	71.0			L-F	80.9								
RHS17	5.9	68.8			S	218.7								
RHS19	3.4	67.7			F	223.9								

US	EXP						FEM						FE / Exp	
			Bif.		Failure			Bif.		Failure			Bif.	Fail.
Spec.	$\Delta\sigma$	E_c	Md.	N_{cr}	Md.	N_u	E_c	Md.	N_{cr}	Md.	N_u	N_t	Bif.	Fail.
US01	2.5	68.8			L-T	31.0	69.3	L	78.4	F	29.4			0.95
US02	9.3	72.3	L	23.8	F	40.6	62.4	L	23.5	L	40.0		0.99	0.98
US04	5.5	67.6	L	24.9	L	40.8	63.2	L	24.4	L	40.3		0.98	0.99
US05	3.7	68.4			L-F	38.4	69.1	L	52.5	L	35.1			0.91
US06	14.5	68.7	L	27.1	L	39.0	69.2	L	28.7	L	38.1		1.06	0.98
US08	4.2	71.1	L	28.6	L	38.8	68.9	L	26.4	L	36.4		0.92	0.94
US10	5.9	67.2			L-F	43.1	69.3	L	43.0	L	38.8			0.90
US11	1.4	65.3			F	33.9	69.5	F	37.0	F	33.5			0.99
US13	4.0	67.6			F	52.4	66.6	F	212.0	F	51.2			0.98
US14	4.0	70.0			D-T	110.6	66.7	L	166.8	L-T	108.2			0.98
US17	11.5	65.5			D-T	71.1	66.7	T	285.9	T	67.0			0.94
US18	8.1	67.6			D-T	99.2	66.7	L	210.5	L	95.7			0.96
US20	9.8	69.8			D-T	98.5	66.8	L	205.0	L-T	96.2			0.98
US21	37.5	63.4			F	66.0	51.0	F	103.2	F	65.7			1.00
US22	6.4	62.8			F	92.4	66.9	L	301.0	L-F	89.4			0.97
US25	22.3	68.4			D-T	59.8	66.0	L	147.2	L-T	56.2			0.94
US26	14.8	68.8	L	59.3	L	74.1	65.2	L	58.5	L	72.8		0.99	0.98
US29	29.5	69.7			L	67.7	66.1	L	106.0	L	64.4			0.95
US30	30.5	65.2	L	61.6	L	71.5	66.1	L	67.2	L	69.7		1.09	0.97
US33	7.5	62.9			F	73.6	66.3	L-F	90.8	L-F	67.1			0.91
US34	10.5	61.9			L-F	77.3	65.8	L	92.2	L-F	75.5			0.98

S = Squashing / L = Local buckling / D = Distortional buckling / F = Flexural buckling / T = Torsional buckling

Table 4-1   Comparison of experimental and FE-results – RHS and US-specimens

CS	EXP						FEM						FE / Exp	
			Bif.		Failure			Bif.		Failure			Bif.	Fail.
Spec.	$\Delta\sigma$	E_c	Md.	N_{cr}	Md.	N_u	E_c	Md.	N_{cr}	Md.	N_u	N_t		
CS01-1	2.2	63.6	L	22.7	F-T	33.8	65.5	L	22.7	FT	32.9		1.00	0.97
CS01-2	4.9	64.1	L	23.6	F-T	36.5	65.5	L	22.7	FT	32.9		0.96	0.90
CS02-1	0.8	63.6			F	65.6	64.5	L	76.0	L	67.9			1.03
CS02-2	3.1	63.2			L	65.4	64.5	L	76.0	L	67.9			1.04
CS02-3	3.0	64.7			F	64.8	64.4	L	75.6	L	66.7			1.03
CS02-4	1.0	63.1			F	64.5	64.4	L	75.6	L	66.7			1.03
CS03-1	7.0	60.4	L	32.2	L	68.4	65.3	L	32.8	L	73.5		1.02	1.07
CS03-2	7.0	66.5	L	29.7	L	68.7	65.3	L	32.8	L	73.5		1.10	1.07
CS03-3	2.7	62.3	L	31.2	L	66.6	65.3	L	32.5	L	72.0		1.04	1.08
CS04-1	25.5	59.7			F-T	36.1	64.7	L	30.9	L	39.1			1.08
CS04-2	11.5	61.9			F-T	34.9	64.7	L	30.9	L	35.7			1.02
CS04-3	4.9	65.2			L	29.8	64.6	FT	29.8	FT	28.1			0.94
CS04-4	19.6	70.7	L/T	18.6	L	21.8	64.6	FT	20.1	FT	23.6	21.7	1.08	0.99
CS05-1	1.8	64.8			D-F	39.3	65.6	D	45.9	D	38.4			0.98
CS05-2	19.3	63.1			D-F	38.0	65.6	D	45.9	D	38.4			1.01
CS05-3	5.5	63.7			D-F	39.3	65.6	D	43.1	D	37.2			0.95
CS06-1	6.6	66.1	L	29.0	F-T	43.2	65.2	L	29.9	L	44.5		1.03	1.03
CS06-2	6.7	62.2	L	26.6	F-T	40.5	65.1	L	29.8	L	43.5		1.12	1.07
CS06-3	12.0	59.6	L	26.4	F-T	38.7	65.0	L	29.6	L	40.9		1.12	1.06
CS06-4	7.1	59.7	FT	25.7	L	28.2	65.2	FT	28.8	FT	32.1	28.8	1.12	1.02
CS07-1	5.0	66.4			F	35.1	66.5	D	42.0	F	37.5			1.07
CS07-2	28.1	60.8	D	34.5	F	36.4	66.5	D	42.0	F	37.5		1.22	1.03
CS08-1	18.2	60.2			L	94.7	67.0	L	95.4	L	95.6			1.01
CS08-2	16.7	60.1			L	93.4	67.0	L	95.4	L	95.6			1.02
CS08-3	3.5	63.3			L	96.0	65.7	L	94.7	L	95.5			1.00
CS09-1	1.9	78.5	L	47.4	L	76.5								
CS09-2	8.5	91.8	L	51.7	L	77.9								
CS09-3	3.0	80.1	L	48.2	L	79.5								
CS10-1	8.9	66.5	L	43.4	F	58.9	68.8	L	44.2	L	61.4		1.02	1.04
CS10-2	5.1	68.1	L	44.5	F	59.3	68.8	L	44.2	L	61.4		0.99	1.04
CS10-3	9.4	68.8	L	47.0	F	55.6	68.7	L	43.8	L	59.8		0.93	1.08
CS10-4	26.2	66.4	L	44.7	F	58.0	68.7	L	43.8	L	58.1		0.98	1.00
CS11-1	2.7	64.2	T	6.7	L	10.4	64.3	T	6.7	T	10.7		1.01	1.03
CS11-2	1.9	64.2	T	5.8	L	10.3	64.6	T	6.1	T	10.3	10.3	1.06	1.00
CS11-3	0.1	64.3	T	5.9	L	9.6	67.1	T	5.9	T	9.6	9.5	1.00	0.99
CS11-4	3.8	63.9	T	5.8	L	8.8	64.6	T	5.7	T	8.6	8.4	0.99	0.96
CS12-1	19.5	62.3	L	13.1	D	30.2	62.5	L	13.7	D	29.2	28.5	1.04	0.94
CS12-2	25.2	48.9	L	10.9	D	29.6	63.9	L	14.8	L	35.0	33.5	1.36	1.13
CS12-3	11.0	62.9	L	12.2	D	28.7	61.9	L	13.6	D	28.8		1.11	1.00
CS12-4	19.0	64.0	L	12.4	D	27.8	60.7	L	13.5	D	28.2		1.09	1.02

S = Squashing / L = Local buckling / D = Distortional buckling / F = Flexural buckling / T = Torsional buckling

Table 4-2   Comparison of experimental and FE-results – CS-specimens

4.2 Comparison of bifurcation and failure loads

The most practical approach to compare the experimental and FE-results of the previous paragraph, is to present them in the non-dimensionalised form of figure 17. This figure presents for each of the test specimens the ultimate load (N_u) divided by the squash load $N_{0.2}$ (=$A f_{0.2}$). The horizontal axis refers to the experiments; the vertical axis, to the finite element results. In addition, the figure includes the unity line that coincides with zero deviation, as well as a 10% upper and lower limit. The following remarks are made:

• The accuracy of the FE-results is good, as comparison of FE results to the experimental results gives an average of μ =1.00 and a standard deviation of σ = 0.06, when considering all specimens. Notably, the largest deviations occur for specimens of which the experiments are considered less accurate.

• The CS-specimens show a larger scatter than the RHS and US-specimens. This is attributed to the complex geometry and the limited plate thickness (1.0 mm).

• Load eccentricity ($\Delta\sigma$) generally results in a constant bending moment in the elastic range. In most cases, the eccentricity is limited to $\Delta\sigma < 20$ N/mm². Experiments with larger load eccentricities result in values of $N_{u;exp}$ less than that of the FE-analyses.
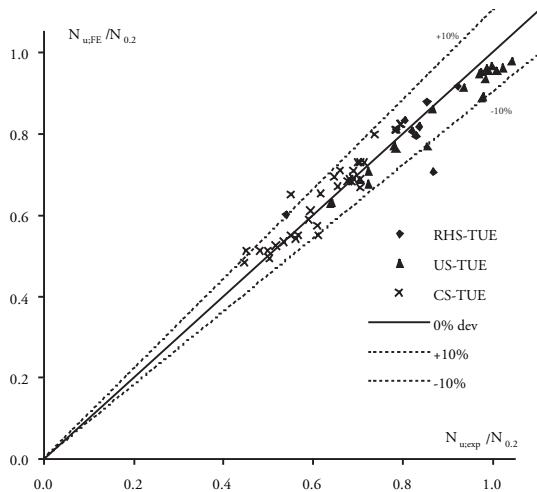

Figure 17: Comparison of experimental and FE-results – Ultimate loads

To obtain insight in the accuracy of the predicted buckling behaviour, figure 18 compares the elastic critical load of the Euler analysis ($N_{cr;FE}$) to the bifurcation load ($N_{cr;exp}$) as observed in the experiments. However, as the elastic critical load is meaningless in the inelastic range, the critical load ($N_{cr;FE}$) is limited to the squash load ($N_{0.2}$) of the respective specimen. Flexural buckling as well as inelastic local buckling will lead to immediate failure, see e.g. figure 14. Therefore, if bifurcation is not observed in the experiments ($N_{cr;exp}$), the failure load is taken

instead ($N_{u;exp}$). The subsequent results are presented in figure 18. The accuracy of the determined bifurcation loads is obviously limited. Nevertheless, the comparison shows a reasonable correlation ($\mu = 1.06$; $\sigma = 0.09$).
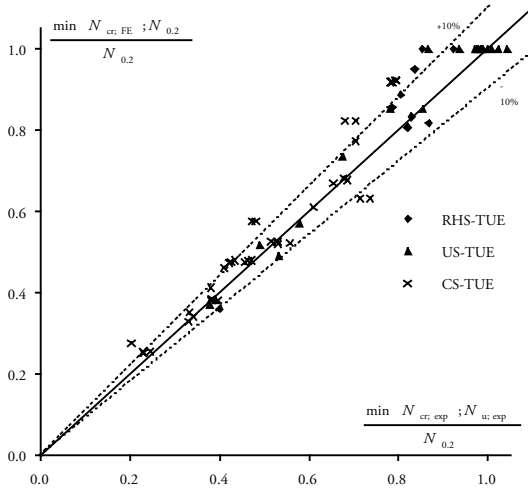

Figure 18: Comparison of experimental and FE-results – Bifurcation loads

5   Conclusions and recommendations

5.1 Conclusions

The following conclusions can be drawn from the comparison of experimental and FE-results:

• A substantial amount of new (experimental and numerical) test data for overall and cross-sectional stability of aluminium extrusions with square hollow sections, U-shaped sections and complex sections is presented.

• The FE-analyses result in deformation modes that coincide with those observed in the experiments.

• The load-displacement diagrams show three types of behaviour: (1) squashing, (2) flexural and flexural-torsional buckling, and (3) local and distortional buckling. The actual behaviour due to squashing highly depends on the material characteristic and support conditions. Overall buckling can be attributed to flexural and flexural-torsional buckling. Failure occurs suddenly and depends highly on "small" inaccuracies of geometry and test set-up. The observed influence of initial deflections was negligible and less than that of the numerically applied ones. The buckling and post-buckling behaviour of local and distortional buckling is well described and the influence of both imperfections and inelastic material is less than that observed for squashing and sudden failure.

- The tangent stiffness of the FE-analyses is identical to that of the input material characteristic. Generally, these coincide with the results of the strain gauges as well. The stiffness of the LVDT is in most cases less, which can be attributed to the influence of the support conditions and loading inaccuracies.
- Load eccentricity generally results in a constant bending moment in the elastic range. In most cases, the resulting eccentricity is limited.
- The FE-analyses accurately predict the ultimate load of the experiments. The bifurcation or critical load is reasonably well predicted, though for obvious reasons less accurate.

5.2 Recommendations

The following recommendations are given:

- Future research should investigate even more complex cross-sectional shapes and their buckling phenomena. It is essential to develop a solid experimental database.
- On the basis of the test results and numerical work presented here, a generally applicable prediction model for the ultimate load of (complex) aluminium sections under compression should be developed. In fact, such a model is already proposed in Mennink (2002).
- Despite the effort taken, the executed experiments are not perfect. Therefore, it is advised to develop an approach that allows the validation of future prediction models and design rules to be based on FE-results, supported by a limited number of experiments.

References

A substantial amount of literature has been reviewed and used, as specified in Mennink (2002). However, the following references contain specific details with respect to the presented results:

[1]   CEN (1993), Design of steel structures, Eurocode 3, Part 1.1, ENV 1993-1-1, Brussels, Belgium

[2]   CEN (1999), Design of aluminium structures, Eurocode 9, Part 1.1, ENV 1999-1-1, Brussels, Belgium

[3]   Hassinen, P. (2000), Compression strength of aluminium columns – Experimental and numerical studies, In: Proceedings of the 3rd International Conference on Coupled Instabilities of Metal Structures, CIMS'2000 (Eds. Camotim D.; Dubina, D.; Rondal J.), ICP, London, UK

[4] Landolfo, R.; Piluso, V.; Langseth, M.; Hopperstad, O.S. (1999), EC9 provisions for flat internal elements, comparison with experimental results, In: Lightweight Steel and Aluminium Structures (Eds. Mäkeläinen, P.; Hassinen, P.), Espoo, Finland

[5] Mazzolani, F.M.; Faella, C.; Piluso, V.; Rizzano, G. (1998), Local buckling of aluminium members: Experimental analysis and cross-sectional classification, Department of Civil Engineering, University of Salerno, Italy

[6] Mennink, J. (2002), Development of a general prediction model for cross-sectional instability of aluminium extrusions with complex cross-sectional shapes, BCO-Report 02.16, Eindhoven University of Technology, Eindhoven (TNO-report 2002-BC-R0038, TNO Building and Construction Research, Delft), The Netherlands

[7] Mennink, J (2002) Cross-sectional stability of aluminium extrusions, Eindhoven, ISBN 90-386-1546-9, The Netherlands. Available at www.tueindhoven.nl

[8] NNI (1991), Metalen – Trekproef, Deel 1: Beproevingsmethode (bij omgevingstemperatuur), NEN 10002-1, Nederlands Normalisatie Instituut, Delft, The Netherlands

[9] Witte, F. de et al (1996), DIANA Finite Element Analysis, User's Manual release 7.2, TNO Building and Construction Research, Delft, The Netherlands